Magnetic signature of the lunar South Pole-Aitken Basin: Character, origin, and age

Michael E. Purucker,[1] and James W. Head III,[2] and Lionel Wilson[3]

Abstract. A new magnetic map of the Moon, based on Lunar Prospector (LP) magnetometer observations, sheds light on the origin of the South Pole-Aitken Basin (SPA), the largest and oldest of the recognized lunar basins. A set of WNW-trending linear to arcuate magnetic features, evident in both the radial and scalar observations, covers much of a 1000 km wide region centered on the NW portion of SPA. The source bodies are not at the surface because the magnetic features show no first-order correspondence to any surface topographic or structural feature. Patchy mare basalts of possible late Imbrian-age are emplaced within SPA and are inferred to have been emplaced through dikes, directly from mantle sources. We infer that the magnetic features represent dike swarms that served as feeders for these mare basalts, as evident from the location of the Thomson/Mare Ingenii, Van de Graaff, and Leeuwenhoek mare basalts on the two largest magnetic features in the region. Modeling suggests that the dike zone is between 25 and 50 km wide at the surface, and dike magnetization contrasts are in the range of 0.2 A/m. We theorize that the basaltic dikes were emplaced in the lunar crust when a long-lived dynamo was active. Based on pressure, temperature, and stress conditions prevalent in the lunar crust, dikes are expected to be a dominantly subsurface phenomenon, consistent with the observations reported here.

1. Introduction

The mapping of magnetic fields has proven to be a useful tool for providing a third dimension to surface observations of the Earth's composition and geologic structure. A suite of mathematical techniques has been developed [*Blakely*, 1995] to facilitate the interpretation of these fields. Application of these techniques to the Moon may permit new insights into the geologic processes acting there.

The magnetic anomalies of the South Pole-Aitken (SPA) basin region have previously been interpreted to be related to impact shock effects in a transient magnetic field by virtue of their locations approximately antipodal to the Imbrium, Serenitatis, and Crisium basins [*Hood et al.*, 2001; *Hood and Artemieva*, 2008].

Magnetic anomalies on the Earth are often the consequence of igneous activity, with the magnetic signal locked in as the magnetic minerals cool below their Curie temperature. An abundance of dikes should exist in the crust of the Moon [*Head and Wilson*, 1992], just as on the Earth [*Wilson and Head*, 1981], although we expect that most of these dikes were probably emplaced early in the history of the Moon before compressive stress reached present levels, and most of them reside in the lower crust. On the Moon, eruptive volcanic phases probably originate from dikes directly from mantle sources, without shallow crustal magma reservoirs. Theoretical analyses of the ascent and eruption of magma, combined with observations of shallow dike intrusions and related deformation on the Moon [*Wilson and Head*, 1981; *Head and Wilson*, 1992] suggest that mare basalts were emplaced in blade-like dikes with dimensions of several tens to many hundreds of kilometers length and tens to 250 m width. Dikes tend to approach the surface from depth with a broad convex-upward shape, and magma eruption usually takes place at the point where the convex portion of the dike first intersects the surface. Radiating , arcuate, and linear mafic dike swarms are common in the Earth [*Ernst et al.*, 1996] and these dikes often have recognizable magnetic signatures [*Reeves*, 2000]. One example of a lunar dike (Rima Sirsalis) with a purported magnetic signature has been identified [*Srnka et al.*, 1979; *Head and Wilson*, 1993; *Hood et al.*, 2001]. The recognition of magnetized dikes would imply the existence of a magnetic epoch in the Moon's history, possibly associated with a lunar dynamo. The paucity of examples identified to date may have to do with the absence of a lunar-wide magnetic field for much of its history, and the absence of detailed modeling and analysis of the low-altitude LP data set.

2. Data

Two internal magnetic field models of the Moon [*Purucker and Nicholas*, 2010] developed from LP magnetometer observations are used here. The first model adopts a sequential approach to the modeling of the external and internal magnetic fields, and best preserves original signal amplitudes. We utilize this model to determine the strength of the magnetization required in our forward models. The second model utilizes a harmonic wavenumber correlation approach to independently determined sequential and coestimation models, and is best for feature recognition. This model is shown in Figure 1 and Figure 2. We utilize this model to characterize the magnetic signature of the SPA basin region. The models extend to spherical harmonic degree 170, and coverage is complete over SPA.

The topographic map utilized here (Figure 3) is based on the Lunar Reconnaissance Orbiter laser altimeter and is described in *Smith et al.* [2010]. The outline of SPA is from *Garrick-Bethell and Zuber* [2009], based on topography, iron, and thorium signatures.

The mare pond observations are from *Yingst and Head* [1997] and the extent of the mare ponds are shown there. In

[1]SGT at Planetary Geodynamics Laboratory, Code 698, Goddard Space Flight Center, Greenbelt, MD 20771, USA.
[2]Brown University, Providence, Rhode Island, USA.
[3]Lancaster University, Lancaster, UK.

0148-0227/12/$9.00

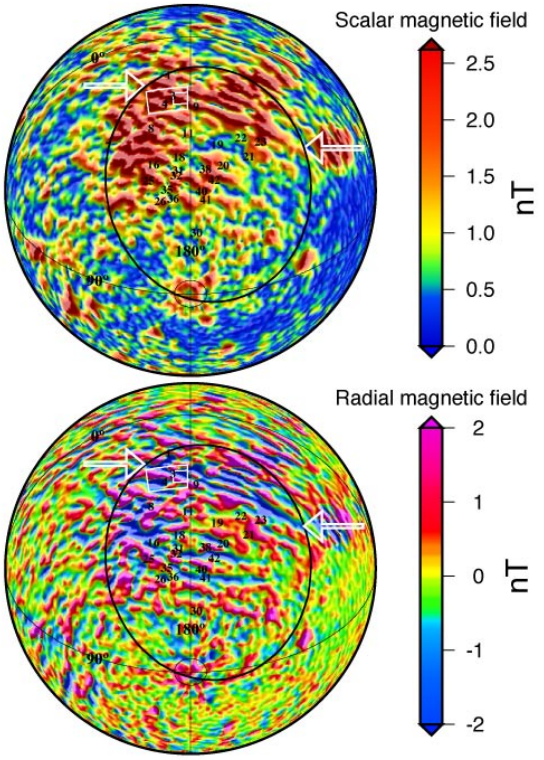

Figure 1. Magnetic maps (scalar at top, radial below) of a region centered on South Pole-Aitken basin (SPA). Magnetic maps at 30 km altitude are based on the harmonic wavenumber correlation map of *Purucker and Nicholas* [2010] using spherical harmonic degrees 1-170. The colored triangles which define the end points of the scale encompass values up to 13 nT for the scalar magnetic field, and range between -13 and 12 nT for the radial magnetic field. Elliptical outline of SPA is from *Garrick-Bethell and Zuber* [2009]. Numbers in and around SPA locate lava ponds greater than 2320 sq km in area. These are further described in Table 1 of *Yingst and Head* [1997], part of which is reproduced here as Table 1. Orthographic projection centered at 180 longitude, 56 South. Illumination is from the north or east. Area shown in Figure 6 is outlined by the small open white rectangle located near the northern edge of the SPA basin, between lava ponds 3 and 9. The larger open white rectangle locates the area of Figure 3 in *Purucker and Nicholas* [2010], and is included here for comparison purposes. The large white arrows define the beginning and end locations of the longest magnetic feature.

our analysis we have retained only lava ponds with areas $\geq$ 2320 sq km (Table 1). This cutoff retains 25 of the original 52 lava ponds. This cutoff was established because it allows for a better matching with the 64 km full wavelength resolution of the global lunar magnetic model [*Purucker and Nicholas*, 2010]. The ultimate resolution of the LP magnetometer data is 9 km along-track [*Purucker and Nicholas*, 2010], a limit set by spin averaging, and comparable to the altitude of the lowest observations.

3. Modeling and Analysis

An overview of the magnetic and topographic framework of the SPA basin is shown in Figure 1, Figure 2, and Figure 3. Overlain on each of these maps are the lava ponds, and the outline of the SPA basin. In order to enhance subtle features in the magnetic and topographic data, Figure 1 and Figure 3 have been enhanced through the use of shaded relief illumination [*Wessel and Smith*, 1998]. The magnetic field observations define a broad area of enhanced magnetic fields centered in the northwestern portion of the SPA basin. Within this region the magnitude and radial magnetic maps clearly delineate WNW-trending magnetic features. One of these features can be seen to extend from one side of the basin to the other, terminating at the ring as defined by *Garrick-Bethell and Zuber* [2009]. The intersection of this 1600 km long feature with the SPA ring is shown with white arrows, and a short segment of this feature was chosen for more detailed modeling, and is outlined by a white rectangle. Shorter WNW-trending magnetic features can be seen in the NE corner of the SPA basin in both the scalar and radial magnetic field maps, with and without shaded relief, and are very clearly evident throughout the NW portion of SPA in the radial magnetic field map. The distribution of large lava ponds follows this same general trend, with concentrations throughout the NW and central portions of the SPA basin. The Thomson/Mare Ingenii mare basalts (8),

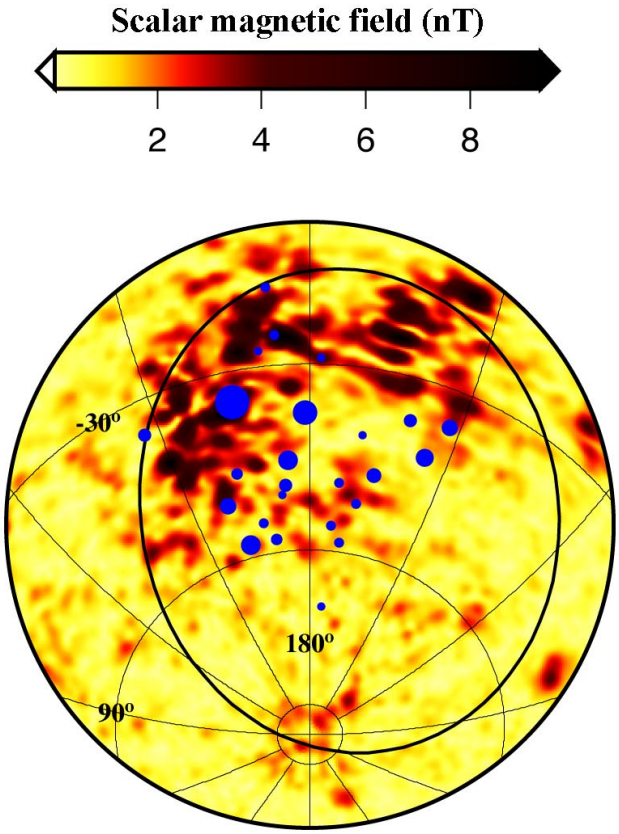

Figure 2. Scalar magnetic field map with the diameter of the largest lava ponds indicated by the size of the blue circle symbol. Area estimates are based on *Yingst and Head* [1997]. Shaded relief illumination is not used for the magnetic field observations. Azimuthal equal area projection centered at 180 longitude, 56 South. Outline of SPA is from *Garrick-Bethell and Zuber* [2009].

by far the largest occurrence by volume (Figure 4) of mare basalts in the SPA region, are located in the middle of the 2nd largest magnetic feature in the region (Figure 4). The Van de Graaff and Leeuwenhoek (3, 4, and 9) mare basalts sit astride the longest and largest (Figure 4) of the magnetic features, as outlined above. In spite of this correspondence, the topographic map (Figure 3) shows little indication of any WNW-trending feature paralleling the magnetic feature. The only suggestion of such a feature is a short segment of the inner ring of SPA in the NE corner of the basin, in an area of enhanced magnetic fields.

The relationship between lava pond volume and the strength of the magnetic field is shown in Figure 4. As previously discussed, several of the lava ponds in the NW corner of SPA have large magnetic anomalies associated with them. The Thomson/Mare Ingenii, Van de Graaff, and Leeuwenhoek lava ponds all have anomalies that exceed the 98th percentile, in terms of the global distribution of lunar magnetic fields. However, the correlation between volume and magnetic magnitude is poor. The Van de Graaff and Leeuwenhoek occurrences have comparatively small volumes, and four other occurrences (7,11,18, and 26) have large volumes but comparatively weak (but still large) magnetic features. With the possible exception of Thomson/Mare Ingenii, this suggests that the lava ponds themselves are insufficient to produce the observed magnetic features.

We now describe the longest magnetic feature (Figure 6 and Figure 5) in the area chosen for detailed study, and describe a forward modeling approach that allows us to estimate parameters of the inferred dike swarm and its magnetization. The Lunar Prospector data set over this region has observations at two altitudes, averaging 22 and 29 km above the lunar datum. Shown in Figure 6 are the locations of the most negative radial magnetic field values along the low (black stars) and high (green stars) altitude passes. This location would identify the center of the source body if it were vertically magnetized. An independent guide to the direction of the magnetization is provided by the difference in the location of the stars at a constant longitude. For a given longitude, the green and black stars would have the same latitude in the case of a vertically magnetized source body. Although there are two sets, at about 174 and 177 degrees longitude, that do not have the same latitude, the correspondence is in general reasonable, so we will assume in our models a vertical magnetization. A linear least-squares fit to these stars (shown in red) delineates the WNW-trending feature, and shows that the largest difference from this line

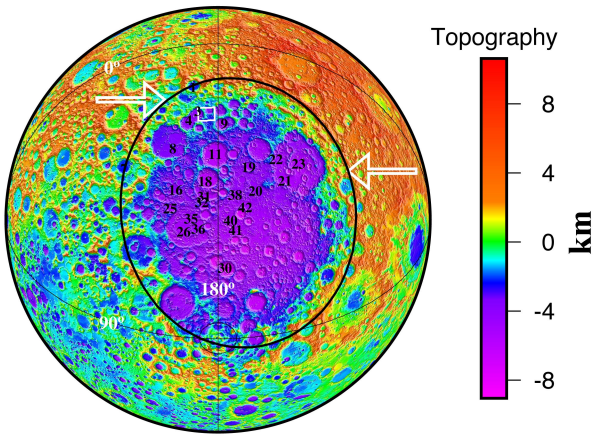

Figure 3. Topographic map of a region centered on South Pole-Aitken basin (SPA). The topographic map is described in *Smith et al.* [2010]. Elliptical outline of SPA is from *Garrick-Bethell and Zuber* [2009]. See Figure 1 for further details.

Table 1. Characteristics of Lava Ponds (Figure 1 and Figure 3) in South Pole-Aitken Basin[a]

Pond	Name	Area (sq. km)	Volume (cu. km)
1	Aitken	3605	1620
3	Van de Graaff NE	3725	745
4	Van de Graaff SW	2455	500
7	Jules Verne	5830	8745
8	Ingenii/Thomson	38140	61025
9	Leeuwenhoek	2320	1055
11	Leibnitz	20500	17425
16	Chrétien	4565	1795
18	Von Kármán	13095	13095
19	Maksutov	2600	1950
20	Nishina E	7815	1565
21	Apollo S	11445	4290
22	Apollo W	5430	2035
23	Apollo N	8335	3125
25	Hopmann	8335	2660
26	Poincaré	13985	9790
30	Antoniadi	2465	495
31	Von Kármán S	5780	4625
32	Poincaré NE	2735	1370
35	Hess	3255	480
36	Poincaré E	4620	2580
38	Nishina SE	3505	1470
40	Bose SW	3540	480
41	Bose S	3135	425
42	Bose N	3610	830

[a] Adapted from *Yingst and Head* [1997], Table 1, showing ponds with areas $\geq$ 2320 sq km.

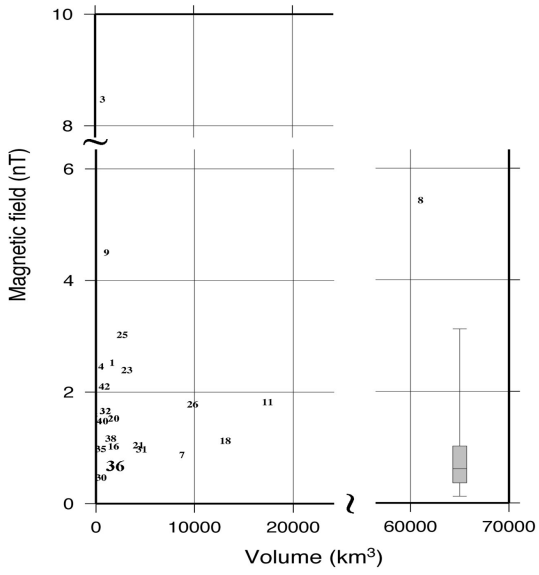

Figure 4. Volume of lava ponds vs magnitude of magnetic field (Figure 1) at 30 km altitude. Numbered lava ponds shown have areas $\geq$ 2320 sq km and are taken from *Yingst and Head* [1997]. Further details are in Table 1. Numbers are keyed to Figure 1. The large number 36 includes 22, and 40 includes 41. A bar and whisker plot of the global magnetic field magnitude at 30 km altitude is also shown. The bottom and top of the gray box are the 25th and 75th percentile, and the band near the middle of the box is the 50th percentile (the median). The ends of the whiskers represent the 2nd and 98th percentile.

occurs in the proximity of the topographic ridge separating the Van de Graaff and Nassau craters. This might be explained if the source bodies were dipping slightly to the SSW.

Stacked profile plots of the B_r and B_θ components of the magnetic field over this area are shown in Figure 5. Because the magnetic features are dominantly oriented E-W, the largest magnetic signatures are expected to be associated with these two components, whereas the E-W component of the magnetic field is expected to be weak, and not diagnostic. We use a two-dimensional approximation to model the magnetic bodies, replacing the cross-sectional shape of the body with an N-sided polygon, in this case a rectangle with width x and depth z as depicted in Figure 7. For uniformly magnetized bodies, the problem then involves the calculation of the magnetic attraction of N flat ribbons of charge [*Blakely*, 1995], infinitely extended in the $+y$ and $-y$ directions, as defined in equations 9.27 and 9.28 of *Blakely* [1995]. See Figure 7 for details of the geometry. It can be shown that the $B_x = -B_\theta$ and $B_z = -B_r$ magnetic fields will be

$$B_x = -2C_m(M \cdot \hat{n})[\hat{s}_x \log \frac{r_2}{r_1} - \hat{s}_z(\theta_1 - \theta_2)] \quad (1)$$

$$B_z = -2C_m(M \cdot \hat{n})[\hat{s}_z \log \frac{r_2}{r_1} + \hat{s}_x(\theta_1 - \theta_2)] \quad (2)$$

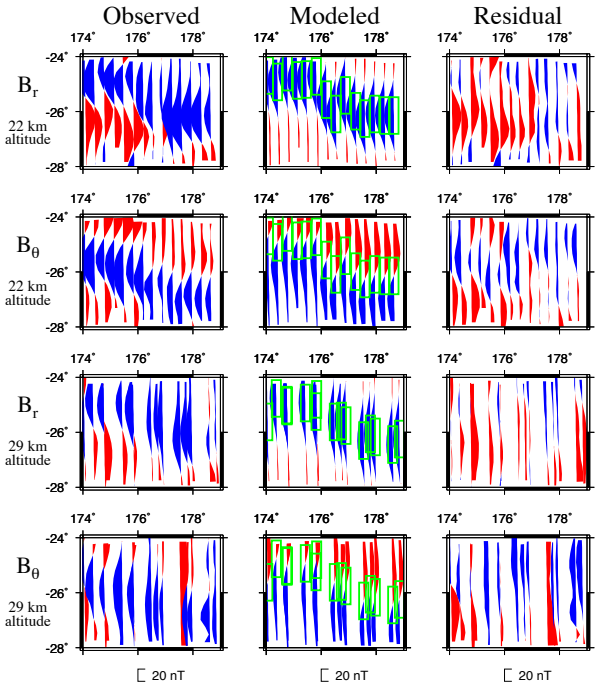

Figure 5. Stacked profile plots show (on the left) the vector magnetic field observations after external field removal ([*Purucker and Nicholas*, 2010]; Sequential approach), the modeled internal component (center), and the remaining unfit field (right). The location is shown in Figure 1 and Figure 6 and is located east of the Van de Graff lava ponds. The two vector components are shown at average altitudes of 22 (range 20–24) and 29 (range 27–31) km. Red colors indicate positive fields, blue are negative. The scale bar below the figures indicates the magnitude of the field. The RMS value for the B_r and B_θ observations at 29 and 22 km is 7.64 nT. After removal of the models, the RMS value decreases to 5.24 nT. The location of the modeled dike swarm is outlined with a green line on the modeling figures.

where r_1 and r_2 are distances from the origin to edges 1 and 2, respectively, and θ_1 and θ_2 are angles between the x-axis and those lines connecting edges 1 and 2, respectively. The vector $\hat{s}$ is always directed parallel to the ribbon from edge 1 to edge 2. C_m is the constant multiplier appropriate for SI units, while $(M \cdot \hat{n})$ describes the magnetization (M) and its direction $(\hat{n})$.

The forward model of a dike swarm [*Wilson and Head*, 1981] that we adopt, shown schematically in Figure 7, has dikes extending from the base of the crust (30 km here, according to the crustal thickness model [*Wieczorek et al.*, 2006]) to the near-surface (0.5 km). An RMS trade-off curve of dike magnetization vs dike zone width (Figure 8), shows that the model that best fits the observations has dike zone widths of 25-50 km at the surface, and magnetizations of between 0.1 and 0.3 A/m. We utilize a dike swarm instead of a single dike in our modeling because rheological constraints [*Head and Wilson*, 1992] suggest that individual dikes are unlikely to be wider than 0.25 km. However, mathematically there is little practical difference between a single dike of magnetization $M/2$ and multiple dikes of magnetization M separated by non-magnetic interlayers of equal width. Using the values selected from the trade-off curve of 0.22 A/m magnetization and a 40 km dike zone thickness, the predicted magnetic field values are calculated and shown in the central panel of Figure 5. The dike zone width of the modeled dikes is shown in green in the central panel of Figure 5, and it should be noted that they are centered on the location of the most negative radial field value (the stars of Figure 6). This might be refined in future work to allow for a continuous dike, if the dike were dipping slightly to the SSW, and if the top of the dike were allowed to follow the lunar topography. After removal of the model from the observations (right panel of Figure 5) the resulting RMS values decrease from 7.6 to 5.2 nT. This RMS misfit is calculated

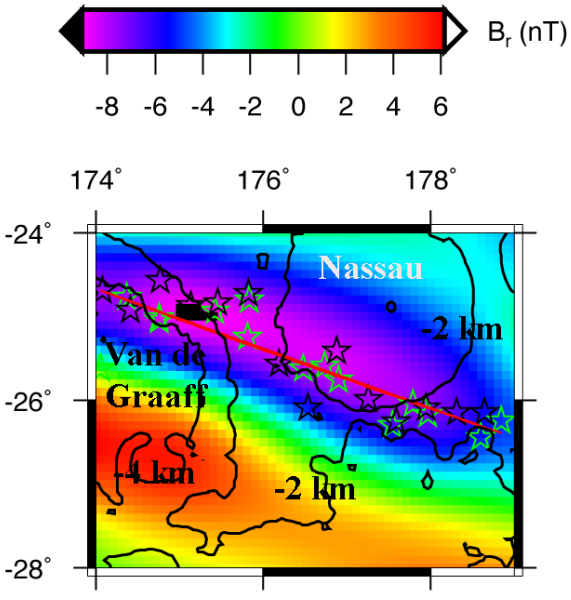

Figure 6. Location of most negative radial field values along low altitude (black stars) and high altitude (green stars) passes shown in Figure 5. Topographic contours in km relative to the lunar datum are shown in solid lines, and the two major basins, Van de Graaff and Nassau are located. The red line is the linear least squares fit to the locations. The radial magnetic field map (Figure 1) is also shown in color as a background. The area shown here is outlined in Figure 1.

between an individual profile and the model. The patterns in the residual misfits suggest the presence of an additional short dike segment in the SW portion of the modeled region with a different, possibly antiparallel, magnetization direction. Assuming a different magnetization direction could affect the magnitude of the predicted magnetizations by as much as a factor of two. However, a different magnetization direction would change the magnetic field pattern and so should be recognizable in the analysis.

4. Discussion

The proximity of these magnetic lineations to the South Pole-Aitken basin suggests that the lineations may be related to the formation of the basin or its subsequent history. Preservation of magnetic fabric dating from early crustal formation processes seems unlikely, due to the physical disruption of crustal target material by the impact and the likelihood that the event would tend to demagnetize and destroy magnetic lineation coherency in the immediate vicinity of the impact. Subsequent to the formation of the South Pole-Aitken basin, the major events in the history are the formation of additional craters and small basins in the basin interior and rim (e.g., Poincaré, Antoniadi, Apollo, Van de Graaff, Aitken and many others) and the formation of the Orientale basin to the east and deposition of Orientale ejecta and crater chains in the interior of SPA [e.g., [*Stuart-Alexander*, 1978; *Wilhelms et al.*, 1979; *Wilhelms*, 1987]. Emplacement of mare basalts on the SPA basin floor occurred well after basin formation and thus mare basalt eruptions tended to pond within the many craters that formed between the time of the impact and the volcanic flooding, and in other low-lying intercrater areas. Unlike the larger nearside maria, such as Imbrium and Serenitatis, which are characterized by widespread, continuous and thick mare deposits (e.g., [*Head and Wilson*, 1992; *Wilhelms*, 1987]), SPA is incompletely flooded and has a patchy mare distribution. *Yingst and Head* [1997] mapped 52 mare ponds in the South Pole-Aitken Basin, with a mean pond area of 2000 sq km, and a mean volume of 860 cubic km. They interpreted the ponds to be due largely to single eruptive phases that were emplaced through dikes directly from mantle sources without shallow crustal magma reservoirs and staging areas.

The timing and strength of the source magnetizations responsible for these magnetic lineations is poorly constrained. *Yingst and Head* [1999] examined the spectral characteristics of 21 of the mare ponds in SPA and found that their affinities were consistent with nearside basalts emplaced in the Late Imbrian Period, a conclusion confirmed by SELENE crater counts [*Haruyama et al.*, 2009]. The possibility also exists for the presence of earlier cryptomaria on the floor of SPA [*Pieters et al.*, 1997]. The recent works of *Garrick-Bethell et al.* [2009] and *Lawrence et al.* [2008] on the lunar sample collection have yielded conflicting interpretations on the question of the existence, timing, and possible strength of a lunar dynamo. We can confidently say only that the Moon may have possessed a surface field of intensity comparable to or smaller than that of the present-day Earth at one or more times in the past, and the favored periods for the existence of a lunar dynamo are the Imbrian, the Nectarian, and the pre-Nectarian. Our knowledge of the expected magnetizations of the basaltic magma from which the dikes originated is also not well known [*Wieczorek and Weiss*, 2010] because it depends on the strength of the magnetizing field, the magnetic mineral responsible for the magnetization, and the amount of iron in the source rocks. *Wieczorek and Weiss* [2010] suggest values between 0.1 and 0.4 A/m for a variety of plausible scenarios, consistent with the values reported here.

Examination of the location of the magnetic lineations shows some positive correlation between their concentration and mare pond locations (Figure 1 and Figure 2). Furthermore, the magnetic lineations cross specific mare ponds in

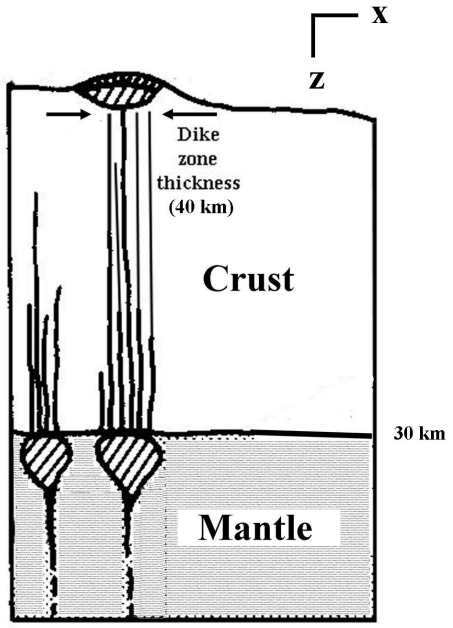

Figure 7. Schematic figure of two dike swarms in the lunar crust, and coordinate system used in the dike geometry problem. The dike is assumed infinite in the $+y$ and $-y$ directions. The dike swarm on the right extends from the base of the crust to the near-surface, where it is shown breaking the surface.

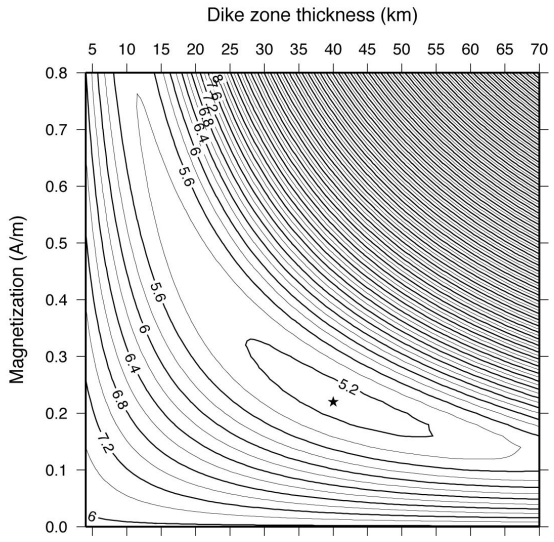

Figure 8. RMS trade-off curve of dike magnetization vs dike zone width. Filled star locates the minimum with magnetization equal to 0.22 A/m and a dike zone thickness (Figure 7) of 40 km, corresponding to 80 dikes each 0.25 km wide, separated from the adjacent dike by a similar width of non-magnetic material. These model parameters are used to calculate the predicted modeled field shown in Figure 5.

some locations. For example, the most prominent linear anomaly trends WNW and crosses mare patches in Van de Graff (3,4), Leeuwenhoek (9), and Apollo (21-23), and trend-parallel graben and mare-related dark-halo craters on the floor of Oppenheimer [*Head et al.*, 2000]. Other linear trends also show correlations with mare patch occurrences. Not all magnetic lineations are associated with mare ponds. In this scenario, not all intrusions reached the surface and resulted in mare ponds. In contrast, all but one of the mare ponds has a magnetic signature greater than the lunar median value, and 18 of the 26 ponds have magnetic signatures above the 75th percentile (Figure 4).

The modeling performed here can not resolve some ambiguities that are inherent in the interpretation of potential field data. For example, because a uniform magnetization can be added to any assumed magnetization distribution with no effect on the measured magnetic field outside [*Runcorn*, 1975; *Purucker and Nicholas*, 2010], it is impossible to distinguish between some plausible geologic scenarios unless samples of the magnetized bodies are available. The satellite is sensitive to only lateral magnetization contrasts. As an example, it is impossible to determine whether the inferred dikes were emplaced in a host rock that was already magnetized, or whether the host rock was non-magnetic.

5. Conclusion

In summary, a number of lines of evidence support an interpretation of the linear magnetic anomalies as the manifestation of magnetized dikes related to the ascent of magma and emplacement of mare basalts on the floor of the South Pole-Aitken basin: 1) the linear nature of the magnetic anomalies and the linear nature of dikes, 2) the concentration of the anomalies in the center and NW portions of the basin where the mare ponds are also concentrated, 3) the coincidence of some magnetic lineation locations with specific basaltic ponds, and 4) the candidate width and depth range of the mare pond feeder dikes and the strength of the magnetic lineations. Thus, we interpret the linear magnetic anomalies to have formed by dikes that emplaced many of the mare ponds on the floor of SPA, with solidification of the dikes taking place in the Late Imbrian, probably 3.6-3.8 Ga, and possibly earlier, during the emplacement of cryptomaria [*Pieters et al.*, 1997].

Future studies of these inferred dike swarms will benefit from the addition of data from the SELENE mission [*Tsunakawa et al.*, 2010] and from higher resolution maps made from LP data (see discussion in [*Purucker and Nicholas*, 2010]). Higher degree gravity field models of the Moon also offer the possibility of independent verification of the dike swarms.

Acknowledgments. Purucker was supported by a NASA Discovery Data Analysis Program contract. GMT [*Wessel and Smith*, 1998] was used for the graphics. We would like to acknowledge the Lunar Prospector team for the collection of this dataset. T. Sabaka, J. Nicholas, N. Tsyganenko, N. Olsen, J. Halekas and M. Acuña provided valuable comments, data sets, or codes. We would also like to acknowledge the JGR editor, and reviewers, for their comments.

References

Blakely, R. (1995), *Potential Theory in Gravity and Magnetic Applications*, Cambridge University Press.

Ernst, R., T. Buchan, T. West, and H. Palmer (1996), Diabase (dolerite) dike swarms of the World: First edition, 1:35000000 scale, *Open-file Report 3241*, Geological Survey of Canada.

Garrick-Bethell, I., and M. Zuber (2009), Elliptical structure of the lunar South Pole-Aitken basin, *Icarus*, *204*, 399–408.

Garrick-Bethell, I., B. Weiss, S. D.L., and J. Buz (2009), Early lunar magnetism, *Science*, *323*, 356–359.

Haruyama, J., et al. (2009), Long-Lived Volcanism on the Lunar Farside Revealed by SELENE Terrain Camera, *Science*, *323*, 905–908.

Head, J., and L. Wilson (1992), Lunar mare volcanism-stratigraphy, eruption conditions, and the evolution of secondary crusts, *Geochim. et Cosmochim. Acta*, *56*, 2155–2175.

Head, J., and L. Wilson (1993), Lunar graben formation due to near-surface deformation accompanying dike emplacement, *Planet. Space Sci.*, *41*, 719–727.

Head, J., L. Wilson, and C. Pieters (2000), Pyroclastic eruptions associated with the floor-fractured lunar farside crater Oppenheimer in the South Pole-Aitken basin, in *Lunar and Planetary Science XXXI*, Abstract #1280, Lunar and Planetary Institute.

Hood, L. L., A. Zakharian, J. Halekas, D. L. Mitchell, R. P. Lin, M. H. Acuña, and A. B. Binder (2001), Initial mapping and interpretation of lunar crustal magnetic anomalies using Lunar Prospector magnetometer data, *J. Geophys. Res.*, *106*, 27,825–27,839.

Hood, L., and N. Artemieva (2008), Antipodal effects of lunar basin-forming impacts: Initial 3-d simulations and comparisons with observations, *Icarus*, *193*, 485–502.

Lawrence, K., C. Johnson, L. Tauxe, and J. Gee (2008), Lunar paleointensity measurements: Implications for lunar magnetic evolution, *Physics of the Earth and Planetary Interiors*, *168*, 71–87.

Pieters, C., S. Tompkins, J. Head, and P. Hess (1997), Mineralogy of the mafic anomaly in the South Pole-Aitken Basin: Implications for excavation of the lunar mantle, *Geophys. Res. Lett.*, *24*, 1903–1906.

Purucker, M., and J. Nicholas (2010), Global spherical harmonic models of the internal magnetic field of the Moon based on sequential and coestimation approaches, *J. Geophys. Res.*, *115*, E12007, doi:10.1029/2010JE003650.

Reeves, C. (2000), The geophysical mapping of Mesozoic dyke swarms in southern Africa and their origin in the disruption of Gondwana, *Journal of African Earth Sciences*, *30*, 499–513.

Runcorn, S. (1975), On the interpretation of lunar magnetism, *Phys.Earth Plan. Int.*, *10*, 327–335.

Smith, D., et al. (2010), Initial observations from the Lunar Orbiter Laser Altimeter (LOLA), *Geophys. Res. Lett.*, *37*, L18204, doi:10.1029/2010GL043751.

Srnka, L., J. Hoyt, J. Harvey, and J. McCoy (1979), A study of the Rima Sirsalis lunar magnetic anomaly, *Physics of the Earth and Planetary Interiors*, *20*, 281–290.

Stuart-Alexander, D. (1978), Geologic map of the central far side of the Moon, *Map I-1047*, U.S. Geological Survey.

Tsunakawa, H., H. Shibuya, F. Takahashi, H. Shimizu, M. Matsushima, A. Matsuoka, S. Nakazawa, H. Otake, and Y. Iijima (2010), Lunar magnetic field observation and initial global mapping of lunar magnetic anomalies by MAP-LMAG onboard SELENE (Kaguya), *Space Science Reviews*, *154*, 219–251.

Wessel, P., and W. Smith (1998), New improved version of Generic mapping tools released, *EOS Trans. AGU*, *79*, 579.

Wieczorek, M., and B. Weiss (2010), Testing the Lunar dynamo hypothesis using global magnetic field data, in *Lunar and Planetary Science XLI*, Abstract #1625, Lunar and Planetary Institute.

Wieczorek, M., et al. (2006), The Constitution and Structure of the Lunar Interior, in *New Views of the Moon*, edited by B. Jolliff, M. Wieczorek, C. Shearer, and C. Neal, pp. 221–364, Mineralogical Society of America.

Wilhelms, D. (1987), *The geologic history of the Moon*, 1348, 302 pp., U.S. Geological Survey.

Wilhelms, D., K. Howard, and W. H (1979), Geologic map of the south side of the Moon, *Map I-1162*, U.S. Geological Survey.

Wilson, L., and J. Head (1981), Ascent and eruption of basaltic magma on the Earth and Moon, *Journal of Geophysical Research*, *86*, 2971–3001.

Yingst, R., and J. Head (1997), Volumes of lunar lava ponds in South Pole-Aitken and Orientale basins: Implications for eruption conditions, transport mechanisms, and magma source regions, *Journal of Geophysical Research*, *102*, 10,909–10,931.

Yingst, R., and J. Head (1999), Geology of mare deposits in South Pole-Aitken basin as seen by Clementine UVVIS data, *Journal of Geophysical Research*, *104*, 18,957–18,979.

Michael E. Purucker, SGT at Planetary Geodynamics Laboratory, Code 698, Goddard Space Flight Center, Greenbelt, MD 20771, USA. (michael.e.purucker@nasa.gov)

James W. Head III, Brown University, Providence, Rhode Island, USA.

Lionel Wilson, Lancaster University, Lancaster, UK.